Aerosol pH and its driving factors in Beijing

Jing Ding[2], Pusheng Zhao[1*], Jie Su[1], Qun Dong[1], Xiang Du[2, 1], and Yufen Zhang[2]

[1] Institute of Urban Meteorology, China Meteorological Administration, Beijing 100089, China

[2] State Environmental Protection Key Laboratory of Urban Ambient Air Particulate Matter Pollution Prevention and Control, College of Environmental Science and Engineering, Nankai University, Tianjin 300071, China

***** *Correspondence to:* P. S. Zhao (pszhao@ium.cn)

Abstract

Aerosol acidity plays a key role in secondary aerosol formation. The high-temporal resolution $PM_{2.5}$ pH and size-resolved aerosol pH in Beijing were calculated with ISORROPIA-II. In 2016-2017, the mean $PM_{2.5}$ pH (at relative humidity (RH) > 30%) over four seasons was 4.5±0.7 (winter) > 4.4±1.2 (spring) > 4.3±0.8 (autumn) > 3.8±1.2 (summer), showing moderate acidity. In coarse-mode aerosols, Ca^{2+} played an important role in aerosol pH. Under heavily polluted conditions, more secondary ions accumulated in the coarse mode, leading to the acidity of the coarse mode aerosols shifted from neutral to weakly acidic. Sensitivity tests also demonstrated the significant contribution of crustal ions to $PM_{2.5}$ pH. In the North China Plain (NCP), the common driving factors affecting $PM_{2.5}$ pH variation in all four seasons were SO_4^{2-}, TNH_3 (total ammonium (gas+aerosol)), and temperature, while the unique factors were Ca^{2+} in spring and RH in summer. The decreasing SO_4^{2-} and increasing NO_3^- mass fractions in $PM_{2.5}$ as well as excessive NH_3 in the atmosphere in the NCP in recent years are the reasons why aerosol acidity in China is lower than that in Europe and the United States. The nonlinear relationship between $PM_{2.5}$ pH and TNH_3 indicated that although NH_3 in the NCP was abundant, the $PM_{2.5}$ pH was still acidic because of the thermodynamic equilibrium between NH_4^+ and NH_3.To reduce nitrate by controlling ammonia, the amount of ammonia must be greatly reduced below excessive quantities.

Key words: Aerosol pH, ISORROPIA-II, Driving factors, Beijing

1. Introduction

Aerosol acidity has a significant effect on secondary aerosol formation through the gas-aerosol partitioning of semi-volatile and volatile species (Eddingsaas et al., 2010; Surratt et al., 2010; Pathak et al., 2011; Guo et al., 2016). Studies have shown that aerosol acidity can promote the generation of secondary organic aerosols by affecting aerosol acid-catalysed reactions (Rengarajan et al., 2011). Moreover, metals can become soluble by acid dissociation under low aerosol pH (Shi et al., 2011; Meskhidze et al., 2003; Fang et al., 2017) or by forming ligands with organic species, such as oxalate, at higher pH (Schwertmann et al., 1991). The investigation of aerosol acidity is conducive to better understanding the important role of aerosols in acid deposition and atmospheric chemical reactions.

Aerosol acidity is frequently estimated by the charge balance of measurable cations and anions. Nevertheless, not all ions (even trace ones) are well constrained in the observations and the dissociation state of multivalent ions are unclear, ion balance and other similar proxies fail to represent the in situ aerosol pH because such metrics cannot accurately predict the H^+ concentration in the aerosol liquid phase (Guo et al., 2015; Hennigan et al., 2015). To better understand the in situ aerosol pH, the aerosol liquid water content (ALWC) and hydrogen ion concentration per volume air (H_{air}^+) should be determined (Guo et al., 2015).

Most inorganic ions and some organic acids in aerosols are water soluble (Peng, 2001; Wang et al., 2017). Since the deliquescence relative humidity (DRH) and the efflorescence relative humidity (ERH) of mixed salts are lower than that of any single component, ambient aerosols are generally in the form of droplets containing liquid water (Seinfeld and Pandis, 2016). ALWC can be derived from hygroscopic growth factors or calculated by thermodynamic models, and good consistencies in ALWC have been found among these methods (Engelhart et al., 2011; Bian et al., 2014; Guo et al., 2015). However, H_{air}^+ can only be obtained by thermodynamic models, which offer a more precise approach to determine aerosol pH (Nowak et al., 2006; Fountoukis et al., 2009; Weber et al., 2016; Fang et al., 2017). Among these thermodynamic models, ISORROPIA-II is widely used owing to its rigorous calculation, performance, and computational speed (Guo et al., 2015; Fang et al., 2017; Liu et al., 2017; Galon-Negru et al., 2018).

The North China Plain (NCP) is the region with the most severe aerosol pollution in China. Nitrate and sulfate are the major contributors to haze, and their secondary formation processes are determined in large part by aerosol pH (Zou et al., 2018; Huang et al., 2017; Gao et al., 2018). Therefore, understanding the aerosol pH level in this region is extremely important and has recently become a trending topic. Fine aerosol pH reported in the NCP (Liu et al., 2017; Song et al., 2018; Shi et al., 2017; Shi et al., 2019) was higher than that found in the United States or Europe, where aerosols are often highly acidic with a pH lower than 3.0 (Guo et al., 2015, 2016; Bougiatioti et al., 2016; Weber et al., 2016; Young et al., 2013). The differences in aerosol pH in the NCP arise from 1) different methods or different model settings, 2) variations in $PM_{2.5}$ chemical composition in the NCP in recent years, 3) the levels of gas precursors of the main water-soluble ions (NH_3, HNO_3, and HCl), and 4) differences in ambient temperature and RH. Studies demonstrated that pH diurnal

variations are largely driven by meteorological conditions (Guo et al., 2015, 2016; Bougiatioti et al., 2016). In the NCP, a comprehensive understanding of the impacts of these factors on aerosol pH is still poor.

Additionally, most studies on aerosol pH focus on PM_1 or $PM_{2.5}$. Knowledge regarding size-resolved aerosol pH is still rare (Fang et al., 2017; Craig et al., 2018). Aerosol chemical compositions are different among multiple size ranges. Among inorganic ions, SO_4^{2-}, NO_3^-, Cl^-, K^+, and NH_4^+ are mainly concentrated in the fine mode except on dusty days (Meier et al., 2009; Pan et al., 2009; Tian et al., 2014), whereas Mg^{2+} and Ca^{2+} are abundant in the coarse mode (Zhao et al., 2017). Aerosol pH can be expected to be diverse among different particle sizes; pH levels at different sizes may be associated with different formation pathways of secondary aerosols.

To better understand the driving factors of aerosol acidity, in this work, the thermodynamic model ISORROPIA-II was utilized to predict aerosol pH in Beijing based on a long-term online high-temporal resolution dataset and a size-resolved offline dataset. The hourly measured $PM_{2.5}$ inorganic ions and precursor gases in four seasons from 2016 to 2017 were used to analyse the seasonal and diurnal variations in aerosol acidity; samples collected by multi-stage cascade impactors (MOUDI-120) were used to estimate the pH variations among 10 different size ranges. Additionally, a sensitivity analysis was conducted to identify the key factors affecting aerosol pH and gas-particle partitioning. The main purposes of this work are to 1) obtain the $PM_{2.5}$ pH level based on an online measurement, contributing towards a global pH dataset; 2) investigate the size-resolved aerosol pH, providing useful information for understanding the formation processes of secondary aerosols; and 3) explore the main factors affecting aerosol pH and gas-particle partitioning, which can help explain the possible reasons for pH divergence in different works and provide a basis for controlling secondary aerosol generation.

2. Data Collection and Methods

2.1 Site

The measurements were performed at the Institute of Urban Meteorology in the Haidian district of Beijing (39°56'N, 116°17'E). The site is located next to a high-density residential area, without significant nearby air pollution emissions. Therefore, the observation data represent the air quality levels of the urban area of Beijing.

2.2 Online data collection

Water-soluble ions (SO_4^{2-}, NO_3^-, Cl^-, NH_4^+, Na^+, K^+, Mg^{2+}, and Ca^{2+}) in $PM_{2.5}$ and gaseous precursors (HCl, HNO_3, HNO_2, SO_2, and NH_3) in ambient air were measured by an online analyser (MARGA) with hourly temporal resolution during spring (April and May 2016), winter (February 2017), summer (July and August 2017), and autumn (September and October 2017). More details about MARGA can be found in Rumsey et al. (2014) and Chen et al. (2017). The $PM_{2.5}$ and PM_{10} mass concentrations (TEOM 1405DF), hourly ambient temperature and RH were also synchronously obtained. The hourly concentrations of $PM_{2.5}$, PM_{10}, and major secondary ions (SO_4^{2-}, NO_3^-, and NH_4^+) in $PM_{2.5}$, as well as meteorological parameters during the observations, are shown

in Figure 1. In the spring, two dust events occurred (April 21 and May 6). In the following pH analysis based on MARGA data, it was assumed that the particles were internally mixed; hence, these two dust events were excluded from this analysis.

Figure 1

2.3 Size-resolved chemical composition

A micro-orifice uniform deposit impactor (MOUDI-120) was used to collect size-resolved aerosol samples with calibrated 50% cut sizes of 0.056, 0.10, 0.18, 0.32, 0.56, 1.0, 1.8, 3.1, 6.2, 9.9 and 18 μm. Size-resolved sampling was conducted July 12-18, 2013; January 13-19, 2014; July 3-5, 2014; October 9-20, 2014; and January 26-28, 2015. Fifteen, fourteen, and eighteen sets of samples were obtained in summer, autumn, and winter, respectively. Except for two sets of samples, all the samples were collected in daytime (from 08:00 to 19:00) and nighttime (from 20:00 to 7:00 the next day). One hour of preparation time was allowed for filter changing and washing the nozzle plate with ethanol. The water-soluble ions in the samples were analysed by using ion chromatography (DIONEX ICS-1000). Detailed information about the features of MOUDI-120 and the procedures of sampling, pre-treatment, and laboratory chemical analysis (including quality assurance & quality control) were described in our previous papers (Zhao et al., 2017; Su et al., 2018).

2.4 Aerosol pH prediction

Aerosol pH can be predicted by thermodynamic models such as AIM and ISORROPIA (Clegg et al., 1998; Nenes et al., 1998). AIM is considered an accurate benchmark model, while ISORROPIA has been optimized for use in chemical transport models. Currently, ISORROPIA-II, with the addition of K^+, Mg^{2+}, and Ca^{2+} (Fountoukis and Nenes, 2007), can calculate the equilibrium H_{air}^+ and ALWC with reasonable accuracy by using the water-soluble ion mass concentration, temperature (T), and RH as input. H_{air}^+ and ALWC were then used to predict aerosol pH by Eq. (1).

$$\mathrm{pH} = -\log_{10} H_{aq}^{+} \cong -\log_{10} \frac{1000 H_{air}^{+}}{ALWC_{i}} \quad (1)$$

where H_{aq}^+ (mole L^{-1}) is the hydronium ion concentration in the ambient particle liquid water. H_{aq}^+ can also be calculated as H_{air}^+ (μg m^{-3}) divided by the concentration of ALWC associated with inorganic species, $ALWC_i$ (μg m^{-3}). Both the inorganic species and part of the organic species in particles are hygroscopic. However, pH prediction is not highly sensitive to water uptake by organic species ($ALWC_o$) (Guo et al., 2015, 2016). In recent years, the fraction of organic matter in $PM_{2.5}$ in the NCP was 20%~25%, which is much lower than that in the United States (Guo et al., 2015). In contrast, approximately 50% of $PM_{2.5}$ in the NCP is inorganic ions (Huang et al., 2017; Zhang et al., 2018; Zhang et al., 2019). The results obtained by Liu et al. (2017) in Beijing showed that the mass fraction of organic matter-induced particle water accounted for only 5% of total ALWC, indicating a negligible contribution to aerosol pH. Hence, aerosol pH can be fairly well predicted by ISORROPIA-II with only measurements of inorganic species in most cases. However, potential errors can be incurred by ignoring $ALWC_o$ in regions where hygroscopic organic species have a relatively high contribution to fine particles.

In ISORROPIA-II, forward and reverse modes are provided to predict ALWC and H_{air}^+. In forward mode, T, RH, and the total (*i.e.*, gas+aerosol) concentrations of NH_3, H_2SO_4, HCl, and HNO_3 need to be input. In reverse mode, equilibrium partitioning is calculated given only the concentrations of aerosol components, RH, and T as input. In this work, the online ion chromatography system MARGA was used to measure both inorganic ions in $PM_{2.5}$ and gaseous precursors. Moreover, the forward mode has been reported to be less sensitive to measurement error than the reverse mode (Hennigan et al., 2015; Song et al., 2018). Hence, ISORROPIA-II was run in forward mode for aerosols in the metastable conditions in this study.

When using ISORROPIA-II to calculate the $PM_{2.5}$ acidity, all particles were assumed to be internally mixed, and the bulk properties were used without considering the variability in chemical composition at a given particle size. In the ambient atmosphere, the aerosol chemical composition is complicated; hence, the deliquescence relative humidity (DRH) of aerosols is generally low (Seinfeld and Pandis, 2016). Once the particles are deliquescent, crystallization only occurs at a very low RH, which is called hysteresis phenomenon. The efflorescence RH (ERH) of a salt cannot be calculated from thermodynamic principles; rather, it must be measured in the laboratory. For a particle consisting of approximately 1:1 $(NH_4)_2SO_4$: NH_4NO_3, the ERH is around 20%, while for a 1:2 molar ratio it decreases to around 10%. (Shaw and Rood 1990). Recently, NO_3^- dominates the particles in the NCP (Zhao et al., 2013, 2017; Huang et al., 2017; Ma et al., 2017); therefore, we assumed that the particles are in a liquid state (metastable condition). Assumption that particles are in metastable were adopted by numerous studies in the NCP (Liu et al., 2017; Guo et al., 2017; Shi et al., 2017; Shi et al., 2019). Figure 2 and Figure S1-S4 show comparisons between the predicted and measured NH_3, HNO_3, HCl, NH_4^+, NO_3^-, Cl^-, $\varepsilon(NH_4^+)$ ($NH_4^+/(NH_3+NH_4^+)$, mol/mol), $\varepsilon(NO_3^-)$ ($NO_3^-/(HNO_3+NO_3^-)$, mol/mol)), and $\varepsilon(Cl^-)$ ($Cl^-/(HCl+Cl^-)$, mol/mol) based on real-time ion chromatography data; all results are coloured with the corresponding RH. The predicted and measured NH_3, NH_4^+, NO_3^-, and Cl^- values are in good agreement: the R^2 values of linear regressions are all higher than 0.94, and the slopes are approximately 1. Moreover, the agreement between the predicted and measured $\varepsilon(NH_4^+)$ is better than those of $\varepsilon(NO_3^-)$ and $\varepsilon(Cl^-)$. The slope of the linear regression between the predicted and measured $\varepsilon(NH_4^+)$ was 0.93, 0.91, 0.95, and 0.96 and R^2 was 0.87, 0.93, 0.89, and 0.97 in spring, winter, summer, and autumn, respectively. However, the measured and predicted partitioning of HNO_3 and HCl show significant discrepancies (R^2 values of 0.28 and 0.18, respectively), which may be attributed to the much lower gas concentrations than particle concentrations, as well as the HNO_3 and HCl measurement uncertainties from MARGA (Rumsey et al., 2014). Clearly, more scatter points deviate from the 1:1 line when ISORROPIA-II is operated at RH≤30%, which is highly evident in winter and spring. It should be noted that when RH is low, ALWC becomes very small, $PM_{2.5}$ pH is subject to considerably more uncertain. Guo et al. (2017) suggest that the lower RH limit is about 40%. In this work, due to the overall good agreement between predictions and measurements when RH was high than 30%,we only determined the $PM_{2.5}$ pH for data with RH higher than 30%.

Figure 2

Running ISORROPIA-II in the forward mode with only aerosol component concentrations as input may result in a bias in predicted pH due to repartitioning of ammonia in the model, leading to a lower predicted pH when gas-phase data are not available (Hennigan et al., 2015). In this work, no synchronous gas phase was available during the MOUDI sampling periods, the gas-phase measurements that were taken by the MARGA in 2017 were therefore applied. Even if the periods are not perfectly aligned, the order of magnitude of NH_3, HNO_3 and HCl during a certain period does not change drastically. Guo et al. (2017) found that even if there is some error in NH_3, pH is less sensitive to it, a factor of 10 change in NH_3 is required to change pH by one unit. Averaged NH_3, HNO_3, and HCl measured by MARGA matched to $PM_{2.5}$ mass concentration levels during the MOUDI sampling periods, together with ion concentrations of samples collected by MOUDI as well as the average RH and T during each sampling period were used to determine the aerosol pH for different size ranges. Similar to calculating the $PM_{2.5}$ pH, it was assumed that all the particles in each size bin were internally mixed and had the same pH.

Comparisons of the measured and predicted NO_3^-, NH_4^+, Cl^- for MOUDI samples are shown in Figure 3. The measured and predicted NO_3^-, NH_4^+, and Cl^- agreed very well in fine-mode particles, the slopes are approximately 1. In the coarse-mode, the predicted NH_4^+ was lower than the measured NH_4^+ due to the impact of crustal ions.

Figure 3

2.5 Sensitivity of $PM_{2.5}$ pH to SO_4^{2-}, TNO_3, TNH_3, Ca^{2+}, RH, and T

To explore the major influencing factors on aerosol pH, sensitivity tests were performed. In the sensitivity analysis, SO_4^{2-}, TNO_3 (total nitrate (gas+aerosol) expressed as equivalent HNO_3), TNH_3 (total ammonium (gas+aerosol) expressed as equivalent NH_3), Ca^{2+}, RH, and T were selected as the variables since SO_4^{2-} and NO_3^- are major anions in aerosols, NH_4^+ and Ca^{2+} are major cations in aerosols, and Ca^{2+} is generally considered representative of crustal ions. To assess how a variable affects $PM_{2.5}$ pH, the real-time measured values of this variable and the average values of other species (K, Na, Mg, and total chloride (gas+aerosol) were also included) in each season were input into ISORROPIA-II. The magnitude of the relative standard deviation (RSD) of the calculated aerosol pH can reflect the impact of variable variations on aerosol acidity. The higher the RSD is, the greater the impact, and vice versa. The average value and variation range for each variable in the four seasons are listed in Table S1.

The sensitivity analysis in this work was only aimed at $PM_{2.5}$ (*i.e.,* fine particles) since the MARGA system equipped with a $PM_{2.5}$ inlet had a high temporal resolution (1 h). In addition, the data set had a wide range, covering different levels of haze events. The sensitivity analysis in this work only reflected the characteristics during the observation periods, and further work is needed to determine whether the sensitivity analysis is valid in other environments.

3. Results and Discussion

3.1 Overall summary of $PM_{2.5}$ pH over four seasons

The average mass concentrations of $PM_{2.5}$ and major inorganic ions in the four seasons are shown in Table 1. Among all the ions measured, NO_3^-, SO_4^{2-}, and NH_4^+ were the three most dominant species, accounting for 83% ~ 87% of the total ion content. The average concentrations of primary inorganic ions (Cl^-, Na^+, K^+, Mg^{2+}, and Ca^{2+}) were higher in spring than in other seasons. $PM_{2.5}$ in Beijing showed moderate acidity, with $PM_{2.5}$ pH values of 4.4±1.2, 4.5±0.7, 3.8±1.2, and 4.3±0.8 for spring, winter, summer, and autumn observations, respectively (data at RH ≤30% were excluded). The overall winter $PM_{2.5}$ pH was comparable to the result (4.2) found in Beijing by Liu et al. (2017) and that (4.5) found by Guo et al. (2017), but lower than that (4.9, winter and spring) in Tianjin (Shi et al., 2017), another mega city approximately 120 km away from Beijing. The $PM_{2.5}$ pH in summer was lowest among all four seasons. The seasonal variation in $PM_{2.5}$ pH in this work was similar to the results in Tan et al. (2018), except for spring, and followed the trend winter (4.11 ± 1.37) > autumn (3.13 ± 1.20) > spring (2.12 ± 0.72) > summer (1.82 ± 0.53).

Table 1

To further investigate the $PM_{2.5}$ pH level under different pollution conditions over four seasons, the $PM_{2.5}$ concentrations were classified into three groups: 0~75 μg m^{-3}, 75~150 μg m^{-3}, and >150 μg m^{-3}, representing clean, polluted, and heavily polluted conditions, respectively. The relationship between $PM_{2.5}$ concentration and pH is shown in Figure S5. The $PM_{2.5}$ pH under clean conditions spanned 2~7, while those under polluted and heavily polluted conditions was mostly concentrated from 3~5. Table 1 shows that as the air quality deteriorated, the aerosol component concentration, as well as ALWC and H_{air}^+, all increased in each season. The average $PM_{2.5}$ pH under clean conditions was the highest (Table 1), followed by polluted and heavily polluted conditions in spring, summer, and autumn. In winter, however, the average pH under polluted conditions (4.8±1.0) was the highest.

On clean days, some higher $PM_{2.5}$ pH values (>6) appeared and were generally accompanied by higher mass fraction of crustal ions (Mg^{2+} and Ca^{2+}). In contrast, lower $PM_{2.5}$ pH (<3) was often accompanied by a higher mass fraction of SO_4^{2-} and lower mass fraction of crustal ions, such conditions were most obvious in summer (Figure 4). Under polluted and heavily polluted conditions, the mass fractions of major chemical components were similar, and the difference in $PM_{2.5}$ pH between these two conditions was also small. All of these results indicated that the aerosol chemical composition should be an essential factor that drives aerosol acidity. The impact of aerosol composition on $PM_{2.5}$ pH is discussed in Section 3.4.

Figure 4

In spring, summer, and autumn, the pH of $PM_{2.5}$ from the northern direction was generally higher than that from the southwest direction, and the higher pH in summer also occurred with strong southwest winds (wind speed >3 m s^{-1}) (Figure 5). Generally, northern winds occur with cold-front systems, which can sweep away air pollutants but raise dust in which the crustal ion species (Ca^{2+}, Mg^{2+}) are higher. In winter, the $PM_{2.5}$ pH was distributed relatively evenly in all wind directions, but we surprisingly found that the pH in northerly winds on clean days could be as low as 3~4,

254 which was consistent with the high mass fraction of SO_4^{2-}.

255 **Figure 5**

256 **3.2 Diurnal variation in ALWC, H_{air}^+, and $PM_{2.5}$ pH**

257 Obvious diurnal variation was observed based on the long-term online dataset, as shown in Figure
258 6. To understand the factors that can drive changes in $PM_{2.5}$ pH, the diurnal variations of NO_3^-, SO_4^{2-},
259 ALWC, and H_{air}^+ were investigated and are exhibited in Figure 6. Generally, ALWC was higher
260 during nighttime than daytime and reached a peak near 04:00 ~ 06:00 (local time). After sunrise,
261 the increasing temperature resulted in a rapid drop in RH, leading to a clear loss of particle water,
262 and ALWC reached the lowest level in the afternoon. H_{air}^+ was highest in the afternoon, followed
263 by nighttime, and H_{air}^+ was relatively low in the morning. The low ALWC and high H_{air}^+ values in
264 the afternoon resulted in the minimum $PM_{2.5}$ pH. The average nighttime pH was 0.3~0.4 units higher
265 than that during daytime. From the above discussion, we found that both H_{air}^+ and ALWC had
266 significant diurnal variations, which means that besides chemical composition, the $PM_{2.5}$ pH diurnal
267 variation was also affected by meteorological conditions. This trend is slightly different from the
268 situation from the US: Guo et al. (2015) found that the ALWC diurnal variation was significant and
269 the diurnal pattern in pH was mainly driven by the dilution of aerosol water.

270 The correlation between NO_3^- concentration and $PM_{2.5}$ pH was weakly positive at low ALWC,
271 and $PM_{2.5}$ pH was almost independent of the NO_3^- mass concentration at higher ALWC values
272 (Figure S6). In contrast, at a low ALWC level, increasing SO_4^{2-} decreased the pH; at a high ALWC
273 level, a negative correlation still existed between SO_4^{2-} mass concentration and $PM_{2.5}$ pH. SO_4^{2-} had
274 a greater effect than NO_3^- on $PM_{2.5}$ pH.

275 **Figure 6**

276 **3.3 Factors affecting $PM_{2.5}$ pH**

277 In this work, the effects of SO_4^{2-}, TNO_3, TNH_3, Ca^{2+}, RH, and T on $PM_{2.5}$ pH were determined
278 through a four-season sensitivity analysis. The common important driving factors affecting $PM_{2.5}$
279 pH variations in all four seasons were SO_4^{2-}, TNH_3, and T (Table 2), while the unique influencing
280 factors were Ca^{2+} in spring and RH in summer. For ALWC, the most important factor was RH,
281 followed by SO_4^{2-} or NO_3^-. Figure 7 and Figure S7-S14 show how these factors affect the $PM_{2.5}$ pH,
282 ALWC, and H_{air}^+ over all four seasons.

283 **Table 2**

284 H_2SO_4 can be completely dissolved in ALWC and in the form of sulfate. As shown in Table 3,
285 HNO_3 also had a high conversion rate to nitrate when RH>30%. Under rich-ammonia conditions
286 (defined and explained in Figure S15), sulfate and nitrate mostly exist in aerosol phase with
287 ammonium. The thermodynamic equilibrium between NH_4^+ and NH_3 makes aerosol acidic (Weber
288 et al., 2016). In the sensitivity tests, we found that elevated SO_4^{2-} is crucial in the increase of H_{air}^+
289 (Figure S7, S9, S12) and ALWC (Figure S8, S10, S13), and has a key role in aerosol acidity (Figure
290 7, S11, S14). However, only the $PM_{2.5}$ pH in winter and autumn decreased significantly with
291 elevated TNO_3 (Figure 7, S14). In spring and summer, $PM_{2.5}$ pH changed little with elevated TNO_3.

Moreover, when the TNO_3 concentration was low, $PM_{2.5}$ pH even increased with elevated TNO_3 (Figure 7, S11). The effect of TNO_3 on H_{air}^+ and ALWC is similar to that of SO_4^{2-}, that is, the elevated TNO_3 will also result in the increase of H_{air}^+ and ALWC. The difference is that SO_4^{2-} can lead to much higher concentration of H_{air}^+ than TNO_3 due to its low volatility (Figure S7, S9, S12). Thus, the sensitivity of $PM_{2.5}$ pH to TNO_3 is less than that to SO_4^{2-}. Moreover, in spring and summer, more excessive NH_3 could continuously react with the increasing TNO_3 (Table S1), leading to the minimal changes in $PM_{2.5}$ pH with elevated TNO_3. Differently, TNH_3 mass concentration was lower in winter and TNO_3 was higher in autumn (Table S1), which made TNH_3 was not excessive enough and resulted in the decreased $PM_{2.5}$ pH with elevated TNO_3.

In the process of increasing NH_3 concentration in the ammonia–nitric acid–sulfuric acid–water system, NH_3 first reacts with sulfuric acid and consumes a large amount of H^+, and then reacts with HNO_3 to produce ammonium nitrate (Seinfeld and Pandis, 2016). After most nitric acid is converted to ammonium nitrate, it is difficult to dissolve more ammonia into aerosol droplet. The sensitivity tests well describe this mechanism. Changes in TNH_3 in the lower concentration range had a significant impact on H_{air}^+ and $PM_{2.5}$ pH, and variations in TNH_3 at higher concentrations could only generate limited pH changes (Figure 7, S11, S14). The nonlinear relationship between $PM_{2.5}$ pH and TNH_3 indicates that although NH_3 in the NCP was abundant, the $PM_{2.5}$ pH was far from neutral.

Figure 7

In this work, $PM_{2.5}$ pH was lowest in summer but highest in winter, which was consistent with the SO_4^{2-} mass fraction with respect to the total ion content. The SO_4^{2-} mass fraction was highest in summer among the four seasons, with a value of 32.4%±11.1%, but lowest in winter, with a value of 20.9%±4.4%. In recent years, the SO_4^{2-} mass fraction in $PM_{2.5}$ in Beijing has decreased significantly due to the strict emission control measures for SO_2; in most cases, NO_3^- dominates the inorganic ions (Zhao et al., 2013, 2017; Huang et al., 2017; Ma et al., 2017), which could reduce aerosol acidity. A study in the Pearl River Delta of China showed that the in situ acidity of $PM_{2.5}$ significantly decreased from 2007-2012; the variation in acidity was mainly caused by the decrease in sulfate (Fu et al.,2015). The excessive NH_3 in the atmosphere and the high NO_3^- mass fraction in $PM_{2.5}$ is the reason why the aerosol acidity in China is lower than that in Europe and the United States (Guo et al., 2017).

Ca^{2+} is an important crustal ion; in the output of ISORROPIA-II, Ca exists mainly as $CaSO_4$ (slightly soluble). Elevated Ca^{2+} concentrations can increase $PM_{2.5}$ pH by decreasing H_{air}^+ and ALWC (Figure 7 and Figure S7-S14). As discussed in Section 3.1, on clean days, $PM_{2.5}$ pH reached 6~7 when the mass fraction of Ca^{2+} was high; hence, the role of crustal ions on $PM_{2.5}$ pH cannot be ignored in areas or seasons (such as spring) in which mineral dust is an important particle source. Due to the strict control measures for road dust, construction sites, and other bare ground, the crustal ions in $PM_{2.5}$ decreased significantly in the NCP, especially on polluted days.

In addition to the particle chemical composition, meteorological conditions also have important impacts on aerosol acidity. RH had different impacts on $PM_{2.5}$ pH in different seasons (Figure 7, S11, S14). In winter, elevated RH could reduce $PM_{2.5}$ pH. However, an opposite tendency was observed in summer. In spring and autumn, RH had little impact on $PM_{2.5}$ pH. Elevated RH can enhance water uptake and promote gas-to-particle conversion, resulting in the increased H_{air}^+ and ALWC synchronously for all four seasons. Therefore, the effect of RH on $PM_{2.5}$ pH depends on the differences in the degree of RH's effect on H_{air}^+ and RH's effect on ALWC. Temperature can alter the $PM_{2.5}$ pH by affecting gas-particle partitioning. At higher ambient temperatures, $\varepsilon(NH_4^+)$, $\varepsilon(NO_3^-)$, and $\varepsilon(Cl^-)$ all showed a decreased tendency (Figure 8, S16). The volatilization of ammonium nitrate and ammonium chloride can result in a net increase in particle H^+ and lower pH (Guo et al., 2018). Moreover, a higher ambient temperature tends to lower ALWC, which can further decrease $PM_{2.5}$ pH.

Figure 8

3.4 Size-resolved aerosol pH

Inorganic ions in particles present clear size distributions, and the size-resolved chemical composition can change at different pollution levels (Zhao et al., 2017; Ding et al., 2017; Ding et al., 2018), which may result in variations in aerosol pH. Thus, we further investigated the size-resolved aerosol pH at different pollution levels. According to the average $PM_{2.5}$ concentration during each sampling period, all the samples were also classified into three groups (clean, polluted, and heavily polluted) according to the rules described in Section 3.1. A severe haze episode occurred during the autumn sampling period; hence, there were more heavily polluted samples in autumn than in other seasons. Figure 9 shows the average size distributions of PM components and pH under clean, polluted, and heavily polluted conditions in summer, autumn, and winter. NO_3^-, SO_4^{2-}, NH_4^+, Cl^-, K^+, OC, and EC were mainly concentrated in the size range of 0.32~3.1 μm, while Mg^{2+} and Ca^{2+} were predominantly distributed in the coarse mode (>3.1 μm). During haze episodes, the sulfate and nitrate in the fine mode increased significantly. However, the increases in Mg^{2+} and Ca^{2+} in the coarse mode were not as substantial as the increases in NO_3^-, SO_4^{2-}, and NH_4^+, and the low wind speed made it difficult to raise dust during heavily polluted periods. More detailed information about the size distributions for all analysed species during the three seasons is given in Zhao et al. (2017) and Su et al. (2018).

Figure 9

The aerosol pH in both fine mode and coarse mode was lowest in summer among the three seasons, followed by autumn and winter. The seasonal variation in aerosol pH derived from MOUDI data was consistent with that derived from the real-time $PM_{2.5}$ dataset. In summer, the predominance of sulfate in fine mode and high ambient temperature resulted in a low pH, ranging from 3.2 to 3.9. The fine-mode aerosol pH in autumn and winter was in the range of 3.9 ~ 5.2 and 4.7 ~ 5.7, respectively. The fine-mode aerosol pH was overall comparable to the $PM_{2.5}$ pH. Moreover, in the fine mode, the difference in aerosol pH among size bins was not significant because the aerosol is

in thermodynamic equilibrium with the gas phase (Fang et al., 2017). Additionally, the size distributions of aerosol pH in the daytime and nighttime were explored and are illustrated in Figure S17. In summer and autumn, the pH in the daytime was lower than that in the nighttime, while in winter, the pH was higher in the daytime. During the winter sampling periods, SO_4^{2-} mass fraction were obviously higher in the nighttime and led to abundant H_{air}^+.

The abundance of Ca^{2+} in the coarse mode led to a predicted aerosol pH approximately at or higher than 7 in autumn and winter. Even if the coarse mode Ca^{2+} mass concentration in the summer was low, the coarse mode aerosol pH was still more than 1 unit higher than the fine mode aerosol pH. The difference in aerosol pH (with and without Ca^{2+}) increased with increasing particle size above 1 μm (Figure S18). Moreover, the coarse-mode aerosols during severely hazy days shifted from neutral to weakly acidic, especially in autumn and winter. As shown in Figure 9, the pH in stage 3 (3.1-6.2 μm) declined from 7.4 (clean) to 5.0 (heavily polluted) in winter. The significant decrease in the mass ratio of Ca^{2+} in the coarse mode particles on heavily polluted days resulted in the loss of acid-buffering capacity. Furthermore, the different size-resolved aerosol acidity levels may be associated with different generation pathways of secondary aerosols. According to Cheng et al. (2017) and Wang et al. (2017), the aqueous oxidation of SO_2 by NO_2 is key in sulfate formation under a high RH and neutral conditions. However, it is speculated that dissolved metals or HONO may be more important for secondary aerosol formation under acidic conditions.

3.5 Factors affecting gas-particle partitioning

Gas-particle partitioning can be directly affected by the concentration levels of gaseous precursors and meteorological conditions. In this work, sensitivity tests showed that decreasing TNO_3 lowered $\varepsilon(NH_4^+)$ effectively, which helped maintain NH_3 in the gas phase. Elevated TNH_3 can increase $\varepsilon(NO_3^-)$ when TNO_3 is fixed, which means that the elevated TNH_3 altered the gas-particle partitioning and shifted more TNO_3 into the particle phase, leading to an increase in nitrate (Figure 8 and S16). Controlling the emissions of both NO_x (gaseous precursor of NO_3^-) and NH_3 are efficient ways to reduce NO_3^-. However, the relationship between TNH_3 and $\varepsilon(NO_3^-)$ in the sensitivity tests (Figure 8 and S16) showed that the $\varepsilon(NO_3^-)$ response to TNH_3 control was highly nonlinear, which means that a decrease in nitrate would happen only when TNH_3 is greatly reduced. The same result was also obtained from a study by Guo et al. (2018). The main sources of NH_3 emission are agricultural fertilization, livestock, and other agricultural activities, which are all associated with people's livelihoods. Therefore, in terms of controlling the generation of nitrate, a reduction in NO_x emissions is more feasible than a reduction in NH_3 emissions.

RH and temperature can also alter gas-particle partitioning. The equilibrium constants for solutions of ammonium nitrate or ammonium chloride are functions of T and RH. The measurement data also showed that lower T and higher RH contribute to the conversion of more TNH_3, TNO_3, and TCl into the particle phase (Table 3). When the RH exceeded 60%, more than 90% of TNO_3 was in the particle phase for all four seasons. In summer and autumn, more than half of the TNO_3 and TCl were partitioned into the gaseous phase at lower RH conditions (≤30%). In winter, low

temperatures favoured the existence of NO_3^- and Cl^- in aerosol phase, and $\varepsilon(NO_3^-)$ and $\varepsilon(Cl^-)$ were higher than 75%, even at low RH. $\varepsilon(NH_4^+)$ was lower than $\varepsilon(NO_3^-)$ and $\varepsilon(Cl^-)$. In spring, summer, and autumn, the average $\varepsilon(NH_4^+)$ was still lower than 0.3 even when the RH was >60%; this trend was associated with excess NH_3 in the NCP. Higher RH and lower temperature are typical meteorological characteristics of haze events in the NCP (Figure 1), which are favourable conditions for the formation of secondary particles.

Table 3.

5. Summary and Conclusions

Long-term high-temporal resolution $PM_{2.5}$ pH and size-resolved aerosol pH in Beijing were calculated with ISORROPIA-II. In 2016-2017 in Beijing, the mean $PM_{2.5}$ pH (RH>30%) over four seasons was 4.5±0.7 (winter) > 4.4±1.2 (spring) > 4.3±0.8 (autumn) > 3.8±1.2 (summer), showing moderate acidity. In this work, both H_{air}^+ and ALWC had significant diurnal variations, indicating that aerosol acidity in the NCP was driven by both aerosol composition and meteorological conditions. The average $PM_{2.5}$ nighttime pH was 0.3~0.4 units higher than that in the daytime. The $PM_{2.5}$ pH in northerly wind was generally higher than that in wind from the southwest. Size-resolved aerosol pH analysis showed that the coarse-mode aerosol pH was approximately equal to or even higher than 7 in winter and autumn, which was considerably higher than the fine mode aerosol pH. The presence of Ca^{2+} had a crucial effect on coarse-mode aerosol pH. Under heavily polluted conditions, the mass fractions of Ca^{2+} in coarse particles decreased significantly, resulting in an evident increase in the coarse mode aerosol acidity. The $PM_{2.5}$ pH sensitivity tests also showed that when evaluating aerosol acidity, the role of crustal ions cannot be ignored in areas or seasons (such as spring) where mineral dust is an important particle source. In northern China, dust can effectively buffer aerosol acidity .

The sensitivity tests in this work showed that the common important driving factors affecting $PM_{2.5}$ pH are SO_4^{2-}, TNH_3, and T, while unique influencing factors were Ca^{2+} in spring and RH in summer. Owing to the significantly rich NH_3 in the atmosphere, the change in $PM_{2.5}$ pH was not significant with the elevated TNO_3, especially in spring and summer. Excess NH_3 in the atmosphere and a high NO_3^- mass fraction in $PM_{2.5}$ is the reason why aerosol acidity in China is lower than that in Europe and the United States. Notably, TNH_3 had a great influence on aerosol acidity at lower concentrations but had a limited influence on $PM_{2.5}$ pH when present in excess. The nonlinear relationship between $PM_{2.5}$ pH and TNH_3 indicated that although NH_3 in the NCP was abundant, the $PM_{2.5}$ pH was still acidic due to the thermodynamic equilibrium between aerosol droplet and precursor gases. Higher ambient temperature could reduce the $PM_{2.5}$ pH by increasing ammonium evaporation and decreasing ALWC. RH had different impacts on $PM_{2.5}$ pH in different seasons, which depends on the differences in the degree of RH's effects on H_{air}^+ and RH's effects on ALWC.

In recent years, nitrates have dominated $PM_{2.5}$ in the NCP, especially on heavily polluted days. Sensitivity tests showed that decreasing TNO_3 and TNH_3 could lower $\varepsilon(NH_4^+)$ and $\varepsilon(NO_3^-)$, helping to reduce nitrate production. However, the $\varepsilon(NO_3^-)$ response to TNH_3 control was highly nonlinear.

Given that ammonia was excessive in most cases, a decrease in nitrate would occur only if TNH_3 were greatly reduced. Therefore, in terms of controlling the generation of nitrate, a reduction in NO_x emissions is more feasible than a reduction in NH_3 emissions.

Data availability. All data in this work are available by contacting the corresponding author P. S. Zhao (pszhao@ium.cn).

Author contributions. P Z designed and led this study. J D and P Z interpreted the data and discussed the results. J S and X D analysed the chemical compositions of size-resolved aerosol samples. J D and P Z wrote the manuscript.

Competing interests. The authors declare that they have no conflict of interest.

Acknowledgements. This work was supported by the National Natural Science Foundation of China (41675131), the Beijing Talents Fund (2014000021223ZK49), and the Beijing Natural Science Foundation (8131003). Special thanks are extended to the Max Planck Institute for Chemistry and Leibniz Institute for Tropospheric Research where Dr. Zhao visited as a guest scientist in 2018.

References

Bian, Y. X., Zhao, C. S., Ma, N., Chen, J., Xu, W. Y.: A study of aerosol liquid water content based on hygroscopicity measurements at high relative humidity in the North China Plain. Atmos. Chem. Phys. 14, 6417-6426, 2014.

Bougiatioti, A., Nikolaou, P., Stavroulas, I., Kouvarakis, G., Weber, R., Nenes, A., Kanakidou, M., Mihalopoulos, N.: Particle water and pH in the eastern Mediterranean: Source variability and implications for nutrient availability, Atmos. Chem. Phys., 16(7), 4579-4591, 2016.

Chen, X., Walker, J. T., and Geron, C.: Chromatography related performance of the Monitor for AeRosols and GAses in ambient air (MARGA): laboratory and field-based evaluation, Atmos. Meas. Tech., 10, 3893-3908, 2017.

Cheng, Y. F., Zheng, G. J., Wei C., Mu, Q., Zheng, B., Wang, Z. B., Gao, M., Zhang, Q., He, K. B., Carmichael, G., Pöschl, U., Su, H.: Reactive nitrogen chemistry in aerosol water as a source of sulfate during haze events in China, Sci. Adv., 2:e1601530, 2016.

Clegg, S. L., et al.: A thermodynamic model of the system H^+, NH_4^+, SO_4^{2-}, NO_3^-, H_2O at tropospheric temperatures, J. Phys. Chem. 102A, 2137-2154, 1998.

Cruz, C. N., Dassios, K. G., Pandis, S. N.: The effect of dioctyl phthalate films on the ammonium nitrate aerosol evaporation rate. Atmos. Environ., 34, 3897-3905, 2000.

Craig, R. L., Peterson, P. K., Nandy, L., Lei, Z., Hossain, M. A., Camarena, S., Dodson, R. A., Cook, R. D., Dutcher, C. S., and Ault, A. P.: Direct determination of aerosol pH: size-Resolved measurements of submicrometer and supermicrometer aqueous particles, Anal Chem, 90, 11232-11239, 10.1021/acs.analchem.8b00586, 2018.

Dassios, K. G., Pandis, S. N.: The mass accommodation coefficient of ammonium nitrate aerosol. Atmos. Environ., 33 (18), 2993-3003, 1999.

Ding, J., Zhang, Y. F., Han, S. Q., Xiao, Z. M., Wang, J., and Feng, Y. C.: Chemical, optical and radiative characteristics of aerosols during haze episodes of winter in the North China Plain, Atmos. Environ., 181, 164-176, 2018.

Ding, X. X., Kong, L. D., Du, C. T., Zhanzakova, A., Fu, H. B., Tang, X. F., Wang, L., Yang, X., Chen, J. M., and Cheng, T. T.: Characteristics of size-resolved atmospheric inorganic and carbonaceous aerosols in urban Shanghai, Atmos. Environ., 167, 625-641, 2017.

Eddingsaas, N. C., VanderVelde, D. G., and Wennberg, P. O.: Kinetics and products of the acid-catalyzed ring-opening of atmospherically relevant butyl epoxy alcohols, J. Phys. Chem. A, 114, 8106-8113, 2010.

Engelhart, G. J., Hildebrandt, L., Kostenidou, E., Mihalopoulos, N., Donahue, N. M., and Pandis, S. N.: Water content of aged aerosol, Atmos. Chem. Phys., 11, 911-920, 2011.

Fang, T., Guo, H. Y., Zeng, L. H., Verma, V., Nenes, A., Weber, R. J.: Highly acidic ambient particles, soluble metals, and oxidative potential: A link between sulfate and aerosol toxicity, Environ. Sci. Technol., 51, 2611-2620, 2017.

Fountoukis, C., and Nenes, A.: ISORROPIA II A computationally efficient aerosol thermodynamic equilibrium model for K^+, Ca^{2+}, Mg^{2+}, NH_4^+, Na^+, SO_4^{2-}, NO_3^-, Cl^-, H_2O aerosols, Atmos. Chem. Phys. 7, 4639-4659, 2007.

Fountoukis, C., Nenes, A., Sullivan, A., Weber, R., Van Reken, T., Fischer, M., Matías, E., Moya, M., Farmer, D., and Cohen, R. C.: Thermodynamic characterization of Mexico City aerosol during MILAGRO 2006, Atmos. Chem. Phys., 9, 2141-2156, 2009.

Fu, X., Guo, H., Wang, X., Ding, X., He, Q., Liu, T., and Zhang, Z.: $PM_{2.5}$ acidity at a background site in the Pearl River Delta region in fall-winter of 2007-2012, J Hazard Mater, 286, 484-492, 2015.

Gao, J. J., Wang, K., Wang, Y., Liu, S. H., Zhu, C. Y., Hao, J. M., Liu, H. J., Hua, S. B., Tian, H. Z.: Temporal-spatial characteristics and source apportionment of $PM_{2.5}$ as well as its associated chemical species in the Beijing-Tianjin-Hebei region of China. Environ. Pollut., 233, 714-724, 2018.

Galon-Negru, A. G., Olariu, R. I., and Arsene, C.: Chemical characteristics of size-resolved atmospheric aerosols in Iasi, north-eastern Romania: nitrogen-containing inorganic compounds control aerosol chemistry in the area, Atmos. Chem. Phys., 18, 5879-5904, 2018.

Guo, H. Y., Sullivan, A. P., Campuzano-Jost, P., Schroder, J. C., Lopez-Hilfiker, F. D., Dibb, J. E., Jimenez, J. L., Thornton, J. A., Brown, S. S., Nenes, A., Weber, R. J.: Fine particle pH and the partitioning of nitric acid during winter in the northeastern United States, J. Geophys. Res. Atmos., 121, 10355-10376, 2016.

Guo, H. Y., Xu, L., Bougiatioti, A., Cerully, K. M., Capps, S. L., Hite Jr., J. R., Carlton, A. G., Lee, S.-H., Bergin, M. H., Ng, N. L., Nenes, A., Weber, R. J.: Fine-particle water and pH in the

520 southeastern United States, Atmos. Chem. Phys., 15, 5211-5228, 2015.
521 Guo, H. Y., Weber, R. J., and Nenes, A.: High levels of ammonia do not raise fine particle pH
522 sufficiently to yield nitrogen oxide-dominated sulfate production, Sci. Rep., 7, doi:
523 10.1038/s41598-017-11704-0, 2017.
524 Guo, H. Y., Otjes, R., Schlag, P., Kiendler-Scharr, A., Nenes, A., and Weber, R. J.: Effectiveness of
525 ammonia reduction on control of fine particle nitrate, Atmos. Chem. Phys., 18, 12241-12256,
526 2018.
527 Hennigan, C. J., Izumi, J., Sullivan, A. P., Weber, R. J., and Nenes, A.: A critical evaluation of proxy
528 methods used to estimate the acidity of atmospheric particles, Atmos. Chem. Phys., 15, 2775-
529 2790, 2015.
530 Huang, X. J., Liu, Z. R., Liu, J. Y., Hu, B., Wen, T. X., Tang, G. Q., Zhang, J. K., Wu, F. K., Ji, D.
531 S., Wang, L. L., Wang, Y. S.: Chemical characterization and source identification of $PM_{2.5}$ at
532 multiple sites in the Beijing–Tianjin–Hebei region, China, Atmos. Chem. Phys., 17, 12941–12962,
533 2017.
534 Liu, M. X., Song, Y., Zhou, T., Xu, Z. Y., Yan, C. Q., Zheng, M., Wu, Z. J., Hu, M., Wu, Y. S., and
535 Zhu, T.: Fine particle pH during severe haze episodes in northern China, Geophys. Res. Lett.,
536 44, 5213-5221, 2017.
537 Ma, Q.X., Wu, Y.F., Zhang, D. Z., Wang, X.J., Xia, Y.J., Liu, X.Y., Tian, P., Han, Z.W., Xia, X.G.,
538 Wang, Y., Zhang, R.J.: Roles of regional transport and heterogeneous reactions in the $PM_{2.5}$
539 increase during winter haze episodes in Beijing, Sci. Total Environ., 599-600, 246-253, 2017.
540 Meier, J., Wehner, B., Massling, A., Birmili, W., Nowak, A., Gnauk, T., Brüggemann, E., Herrmann,
541 H., Min, H., Wiedensohler, A.: Hygroscopic growth of urban aerosol particles in Beijing (China)
542 during wintertime: a comparison of three experimental methods, Atmos. Chem. Phys., 9, 6865–
543 6880, 2009.
544 Meskhidze, N., Chameides, W. L., Nenes, A., and Chen, G.: Iron mobilization in mineral dust: Can
545 anthropogenic SO_2 emissions affect ocean productivity? Geophys. Res. Lett., 30, 2085,
546 doi:10.1029/2003gl018035, 2003.
547 Nenes, A., Pandis, S. N., and Pilinis, C.: ISORROPIA: A new thermodynamic equilibrium model
548 for multiphase multicomponent inorganic aerosols, Aquat Geochem, 4, 123-152, 1998.
549 Nowak, J. B., Huey, L. G., Russell, A. G., Tian, D., Neuman, J. A., Orsini, D., Sjostedt, S. J., Sullivan,
550 A. P., Tanner, D. J., Weber, R. J., Nenes, A., Edgerton, E., Fehsenfeld, F. C.: Analysis of urban
551 gas phase ammonia measurements from the 2002 Atlanta Aerosol Nucleation and Real-Time
552 Characterization Experiment (ANARChE), J. Geophys. Res., 111, D17308,
553 doi:10.1029/2006jd007113, 2006.
554 Pan, X. L., Yan, P., Tang, J., Ma, J. Z., Wang, Z. F., Gbaguidi, A., and Sun, Y. L.: Observational
555 study of influence of aerosol hygroscopic growth on scattering coefficient over rural area near
556 Beijing mega-city, Atmos. Chem. Phys., 9, 7519-7530, 2009.
557 Pathak, R. K., Wang, T., Ho, K. F., Lee, S. C.: Characteristics of summertime $PM_{2.5}$ organic and

elemental carbon in four major Chinese cities: Implications of high acidity for water soluble organic carbon (WSOC), Atmos. Environ., 45, 318-325, 2011.

Peng, C. G., Chan, M. N., and Chan, C. K.: The hygroscopic properties of dicarboxylic and multifunctional acids: Measurements and UNIFAC predictions, Environ. Sci. Technol., 35, 4495-4501, 2001.

Rengarajan, R., Sudheer, A.K., Sarin, M.M.: Aerosol acidity and secondary formation during wintertime over urban environment in western India. Atmos. Environ., 45: 1940-1945, 2011.

Rumsey, I. C., Cowen, K. A., Walker, J. T., Kelly, T. J., Hanft, E. A., Mishoe, K., Rogers, C., Proost, R., Beachley, G. M., Lear, G., Frelink, T., and Otjes, R. P.: An assessment of the performance of the Monitor for AeRosols and GAses in ambient air (MARGA): a semi-continuous method for soluble compounds, Atmos. Chem. Phys., 14, 5639-5658, 2014.

Schwertmann, U., Cornell, R. M.: Iron Oxides In the Laboratory: Preparation and Characterization, Weinheim, WCH Publisher, 1991.

Seinfeld, J. H., Pandis, S. N.: Atmospheric Chemistry and Physics: From Air Pollution to Climate Change (3rd edition), John Wiley & Sons, Inc., Hoboken, New Jersey, USA, 2016.

Shi, G. L., Xu, J., Peng, X., Xiao, Z. M., Chen, K., Tian, Y. Z., Guan, X. P., Feng, Y. C., Yu, H. F., Nenes, A., Russell, A. G.: pH of aerosols in a polluted atmosphere: source contributions to highly acidic aerosol, Environ. Sci. Technol., DOI: 10.1021/acs.est.6b05736, 2017.

Shi, X. R., Nenes, A., Xiao, Z. M., Song, S. J., Yu, H. F., Shi, G. L., Zhao, Q. Y., Chen, K., Feng, Y. C., and Russell, A. G.: High-resolution data sets unravel the effects of sources and meteorological conditions on nitrate and its gas-particle partitioning, Environ. Sci. Technol., 53, 3048-3057, 2019.

Shi, Z., Bonneville, S., Krom, M. D., Carslaw, K. S., Jickells, T. D., Baker, A. R., Benning, L. G.: Iron dissolution kinetics of mineral dust at low pH during simulated atmospheric processing. Atmos. Chem. Phys., 11, 995-1007, 2011.

Song, S. J., Gao, M., Xu, W. Q., Shao, J. Y., Shi, G. L., Wang, S. X., Wang, Y. X., Sun, Y. L., McElroy, M. B.: Fine particle pH for Beijing winter haze as inferred from different thermodynamic equilibrium models. Atmos. Chem. Phys., 18, 7423-7438, 2018.

Su, J., Zhao, P. S., Dong, Q.: Chemical Compositions and Liquid Water Content of Size-Resolved Aerosol in Beijing. Aerosol Air Qual. Res., 18, 680-692, 2018.

Surratt, J. D., Chan, A. W., Eddingsaas, N. C., Chan, M., Loza, C. L., Kwan, A. J., Hersey, S. P., Flagan, R. C., Wennberg, P. O., and Seinfeld, J. H.: Reactive intermediates revealed in secondary organic aerosol formation from isoprene, PNAS. USA, 107, 6640-6645, 2010.

Tan, T. Y., Hu, M., Li, M. R., Guo, Q. F., Wu, Y. S., Fang, X., Gu, F. T., Wang, Y., Wu, Z. J.: New insight into $PM_{2.5}$ pollution patterns in Beijing based on one-year measurement of chemical compositions. Sci. Total Environ., 621, 734-743, 2018.

Tian, S. L., Pan, Y. P., Liu, Z.R., Wen, T. X., Wang, Y. S.: Size-resolved aerosol chemical analysis of extreme haze pollution events during early 2013 in urban Beijing, China. J. Hazard. Mater., 279, 452-460, 2014.

Wang, G., Zhang, R., Gomez, M. E., Yang, L., Levy Zamora, M., Hu, M., Lin, Y., Peng, J., Guo, S., Meng, J., Li, J., Cheng, C., Hu, T., Ren, Y., Wang, Y., Gao, J., Cao, J., An, Z., Zhou, W., Li, G., Wang, J., Tian, P., Marrero-Ortiz, W., Secrest, J., Du, Z., Zheng, J., Shang, D., Zeng, L., Shao, M., Wang, W., Huang, Y., Wang, Y., Zhu, Y., Li, Y., Hu, J., Pan, B., Cai, L., Cheng, Y., Ji, Y., Zhang, F., Rosenfeld, D., Liss, P. S., Duce, R. A., Kolb, C. E., and Molina, M. J.: Persistent sulfate formation from London Fog to Chinese haze, Proc. Natl. Acad. Sci. U.S.A., 113, 13630-13635, 2016.

Wang, X. W., Jing, B., Tan, F., Ma, J.B., Zhang, Y. H., Ge, M.F.: Hygroscopic behavior and chemical composition evolution of internally mixed aerosols composed of oxalic acid and ammonium sulfate, Atmos. Chem. Phys., 17, 12797-12812, 2017.

Weber, R. J., Guo, H., Russell, A. G., Nenes, A.: High aerosol acidity despite declining atmospheric sulfate concentrations over the past 15 years. Nat. Geosci., 9, 282-285, 2016.

Young, A. H., Keene, W. C., Pszenny, A. A. P., Sander, R., Thornton, J. A., Riedel, T. P., Maben, J. R.: Phase partitioning of soluble trace gases with size-resolved aerosols in near-surface continental air over northern Colorado, USA, during winter, J. Geophys. Res. Atmos., 118, 9414-9427, doi:10.1002/jgrd.50655, 2013.

Zhang, H., Cheng, S., Li, J., Yao, S., and Wang, X.: Investigating the aerosol mass and chemical components characteristics and feedback effects on the meteorological factors in the Beijing-Tianjin-Hebei region, China, Environ Pollut, 244, 495-50, 2019.

Zhang, Y., Lang, J., Cheng, S., Li, S., Zhou, Y., Chen, D., Zhang, H., and Wang, H.: Chemical composition and sources of PM_1 and $PM_{2.5}$ in Beijing in autumn, Sci Total Environ, 630, 72-82, 2018.

Zhao, P. S., Chen, Y. N., Su, J.: Size-resolved carbonaceous components and water-soluble ions measurements of ambient aerosol in Beijing. J. Environ. Sci., 54, 298-313, 2017.

Zhao, P. S., Dong, F., He, D., Zhao, X.J., Zhang, X.L., Zhang, W.Z., Yao, Q., Liu, H. Y.: Characteristics of concentrations and chemical compositions for $PM_{2.5}$ in the region of Beijing, Tianjin, and Hebei, China. Atmos. Chem. Phys., 13, 4631-4644, 2013.

Zou, J. N., Liu, Z. R., Hu, B., Huang, X. J., Wen, T. X., Ji, D. S., Liu, J. Y., Yang, Y., Yao, Q., Wang, Y. S.: Aerosol chemical compositions in the North China Plain and the impact on the visibility in Beijing and Tianjin. Atmos. Res. 201, 235-246, 2018.

Table captions

Table 1. Average mass concentrations of NO_3^-, SO_4^{2-}, NH_4^+ and $PM_{2.5}$, as well as ALWC, H_{air}^+, and $PM_{2.5}$ pH, under clean, polluted, and heavily polluted conditions over four seasons.

Table 2. Sensitivity of $PM_{2.5}$ pH to SO_4^{2-}, TNH_3, TNO_3, Ca^{2+}, RH, and T. A larger magnitude of the relative standard deviation (RSD) represents a larger impact derived from variations in variables.

Table 3. Average measured $\varepsilon(NH_4^+)$, $\varepsilon(NO_3^-)$, and $\varepsilon(Cl^-)$ based on the real-time MARGA dataset and ambient temperature at different ambient RH levels in four seasons.

635 **Table 1**

Spring	$PM_{2.5}$	NO_3^-	SO_4^{2-}	NH_4^+	ALWC*	H_{air}^{+*}	pH*
	μg m^{-3}	μg m^{-3}	μg m^{-3}	μg m^{-3}	μg m^{-3}	μg m^{-3}	
Average	57±42	12.6±14.2	8.4±7.7	6.7±7.2	21±33	3.7E-06±1.5E-05	4.4±1.2
Clean	39±19	6.6±6.5	5.4±3.8	3.6±3.2	13±23	3.2E-06±1.9E-05	4.6±1.4
Polluted	101±21	30.7±14.3	16.2±6.2	15.3±6.0	33±36	3.1E-06±2.9E-06	4.1±0.4
Heavily polluted	199±62	36.4±19.8	29.3±14.0	23.2±12.3	78±60	1.6E-05±5.4E-06	3.7±0.3
Winter	$PM_{2.5}$	NO_3^-	SO_4^{2-}	NH_4^+	ALWC*	H_{air}^{+*}	pH*
Average	60±69	13.7±21.0	7.3±8.7	7.3±10.0	35±46	2.2E-05±2.3E-04	4.5±0.7
Clean	22±20	3.6±3.9	2.8±1.8	2.2±2.0	10±16	3.2E-07±4.8E-07	4.5±0.6
Polluted	107±21	18.9±8.6	11.0±5.7	11.0±4.7	41±45	1.9E-05±9.1E-05	4.8±1.0
Heavily polluted	209±39	59.7±21.8	26.2±6.3	29.1±8.7	80±52	7.0E-05±4.7E-04	4.4±0.7
Summer	$PM_{2.5}$	NO_3^-	SO_4^{2-}	NH_4^+	ALWC*	H_{air}^{+*}	pH*
Average	39±24	9.5±9.5	8.6±7.5	7.2±5.6	50±68	1.6E-05±1.8E-05	3.8±1.2
Clean	33±18	7.3±6.8	7.0±6.0	5.9±4.0	42±61	1.4E-05±1.6E-05	3.8±1.2
Polluted	87±13	26.5±10.5	20.7±7.0	17.6±4.8	100±88	3.1E-05±2.0E-05	3.5±0.4
Autumn	$PM_{2.5}$	NO_3^-	SO_4^{2-}	NH_4^+	ALWC*	H_{air}^{+*}	pH*
Average	59±48	18.5±19.5	6.5±5.9	8.2±8.2	109±160	8.1E-06±1.1E-05	4.3±0.8
Clean	33±21	7.6±7.4	4.4±4.1	3.8±3.5	49±83	3.8E-06±6.6E-06	4.5±1.0
Polluted	105±21	33.8±11.6	14.3±6.3	16.0±4.6	225±189	1.7E-05±1.2E-05	4.1±0.3
Heavily polluted	174±18	63.4±15.4	25.0±15.9	29.0±5.1	317±236	2.2E-05±1.0E-05	4.1±0.2

636 * For data with RH>30%.

637

638 **Table 2**

Impact Factor	SO_4^{2-}	TNO_3	TNH_3	Ca^{2+}	RH	T
Spring- RSD	12.4%	5.2%	3.9%	7.5%	1.3%	7.0%
Winter- RSD	28.1%	8.4%	27.0%	1.0%	4.1%	6.7%
Summer- RSD	7.9%	3.6%	8.1%	1.9%	8.6%	5.8%
Autumn- RSD	6.0%	3.3%	16.1%	0.8%	2.4%	7.5%

639

640

641

642 **Table 3**

	RH	T, °C	$\varepsilon(NH_4^+)$	$\varepsilon(NO_3^-)$	$\varepsilon(Cl^-)$
Spring	≤ 30%	24.8 ± 3.7	0.17±0.14	0.84±0.12	0.67±0.24
	30~60%	20.6 ± 3.8	0.25±0.14	0.91±0.06	0.82±0.16
	>60%	15.8 ± 2.7	0.28±0.12	0.96±0.03	0.96±0.06
Winter	≤ 30%	5.4 ± 5.3	0.31±0.13	0.78±0.12	0.89±0.14
	30~60%	1.0 ± 3.6	0.50±0.21	0.89±0.10	0.97±0.03
	>60%	-1.9 ± 2.1	0.60±0.20	0.96±0.03	0.99±0.01
Summer	≤ 30%	35.6± 0.4	0.06±0.02	0.35±0.20	0.39±0.17
	30~60%	29.6 ± 4.2	0.17±0.11	0.65±0.23	0.43±0.16
	>60%	25.2 ± 3.8	0.26±0.12	0.90±0.12	0.71±0.15
Autumn	≤ 30%	21.7± 7.5	0.07±0.06	0.49±0.25	0.45±0.21
	30~60%	20.8± 6.3	0.21±0.14	0.82±0.19	0.67±0.21
	>60%	14.9 ± 5.7	0.30±0.19	0.92±0.10	0.86±0.13

643

644

645

Figure captions

Figure 1. Time series of relative humidity (RH) and temperature (T) (a, e, i, m); $PM_{2.5}$, PM_{10}, and NH_3 (b, f, g, n); dominant water-soluble ions: NO_3^-, SO_4^{2-}, and NH_4^+ (c, g, k, o); and $PM_{2.5}$ pH coloured by $PM_{2.5}$ concentration (d, h, l, p) over four seasons.

Figure 2. Comparisons of predicted and measured NH_3, HNO_3, HCl, NH_4^+, NO_3^-, Cl^-, $\varepsilon(NH_4^+)$, $\varepsilon(NO_3^-)$, and $\varepsilon(Cl^-)$ coloured by RH. In this figure, the data from all four seasons were combined; comparisons of individual seasons are shown in Figure S1-S4.

Figure 3. Comparisons of predicted and measured NH_4^+, NO_3^-, Cl^- coloured by particle size. In this figure, all MOUDI data were combined.

Figure 4. Time series of mass fractions of NO_3^-, SO_4^{2-}, NH_4^+, Cl^-, Mg^{2+}, and Ca^{2+} with respect to the total ion content, as well as $PM_{2.5}$ pH in all four seasons ($PM_{2.5}$ pH values at RH≤30% were excluded).

Figure 5. Wind-dependence map of $PM_{2.5}$ pH over four seasons. In each picture, the shaded contour indicates the mean value of $PM_{2.5}$ pH for varying wind speeds (radial direction) and wind directions (transverse direction) (data at RH≤30% were excluded).

Figure 6. Diurnal patterns of mass concentrations of NO_3^- and SO_4^{2-} in $PM_{2.5}$, predicted aerosol liquid water content (ALWC), H_{air}^+, and $PM_{2.5}$ pH over four seasons. Mean and median values are shown, together with 25% and 75% quantiles. Data at RH≤30% were excluded, and the shaded area represents the time period when most RH values were lower than 30%.

Figure 7. Sensitivity tests of $PM_{2.5}$ pH to SO_4^{2-}, TNO_3, TNH_3, Ca^{2+}, and meteorological parameters (RH and T) in summer (S) and winter (W).

Figure 8. Sensitivity tests of $\varepsilon(NH_4^+)$, $\varepsilon(NO_3^-)$ to TNO_3, TNH_3, RH and T coloured by $PM_{2.5}$ pH in summer (S) and winter (W).

Figure 9. Size distributions of aerosol pH and all analysed chemical components under clean (a, d, g), polluted (b, e, h), and heavily polluted conditions (c, f, i) in summer, autumn, and winter.

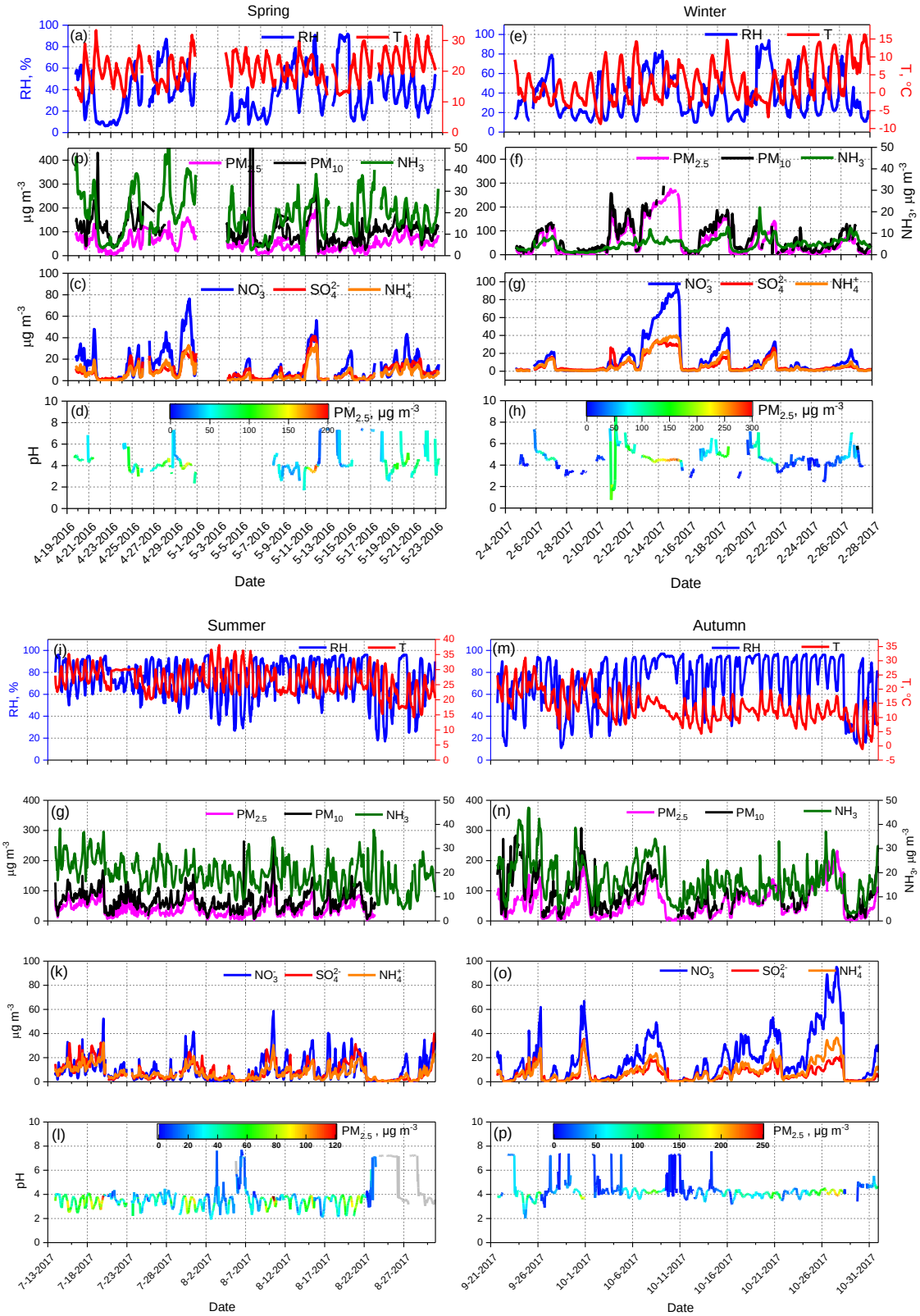
Spring
Winter
Summer
Autumn
RH, %
T, °C
µg m-3
NH3, µg m-3
pH
PM2.5, µg m-3
RH
T
PM2.5
PM10
NH3
NO3-
SO42-
NH4+
Date

Figure 1.

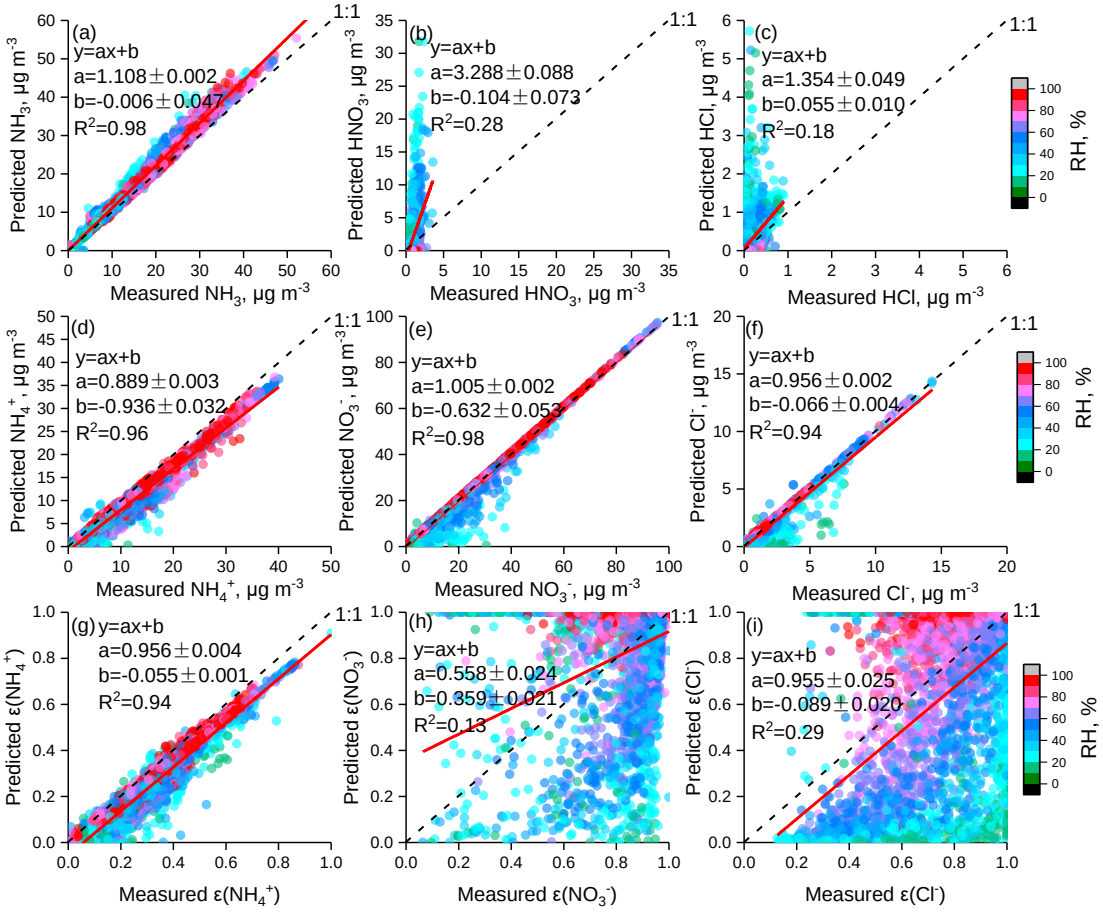

675

676 **Figure 2.**

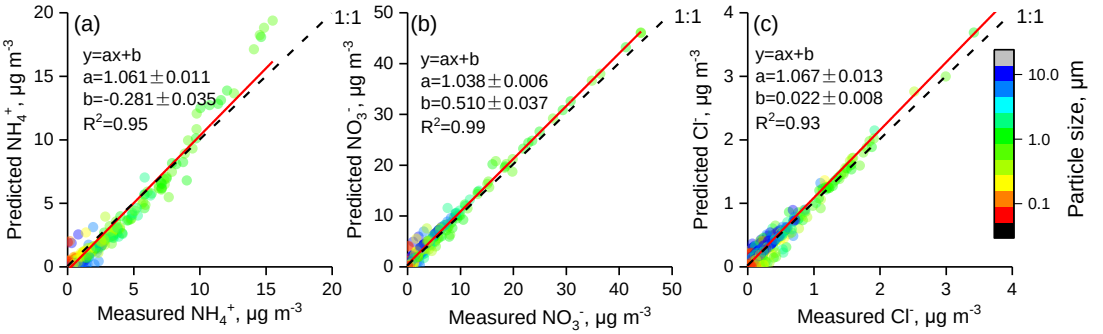

677

678

679 **Figure 3.**

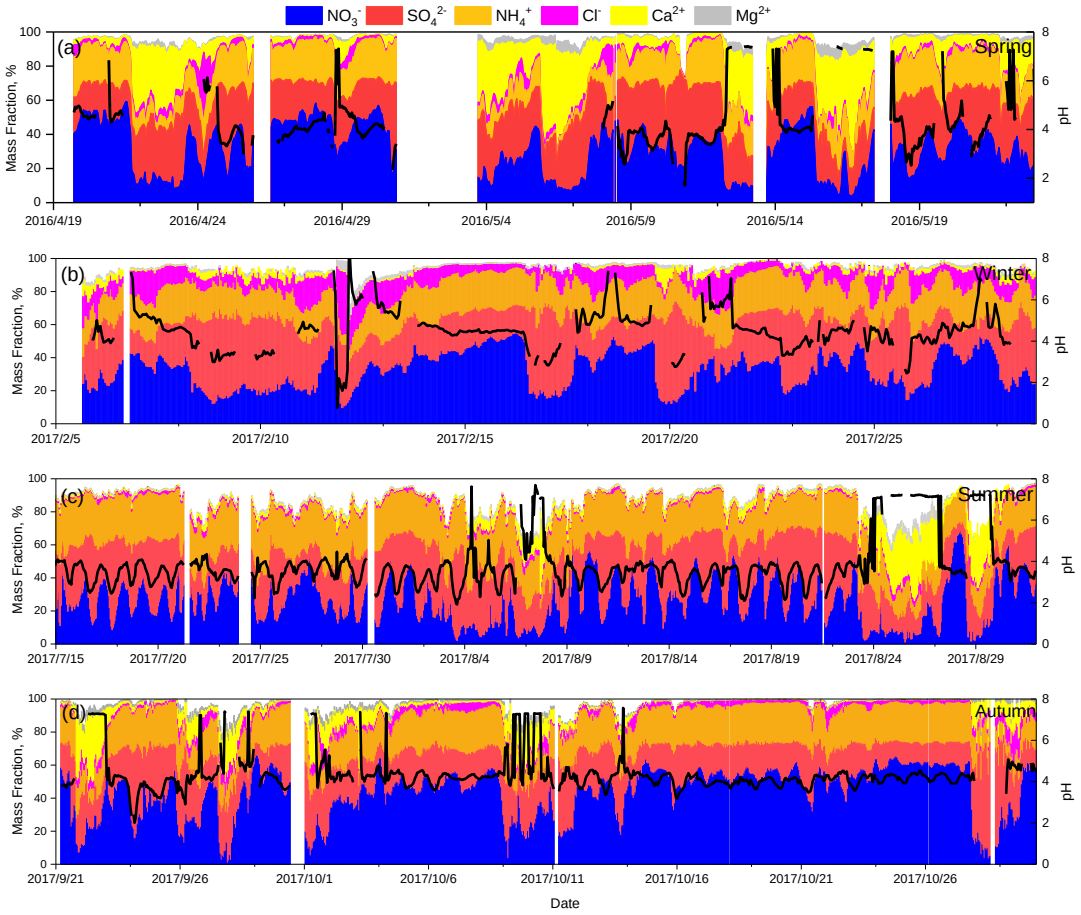

Figure 4.

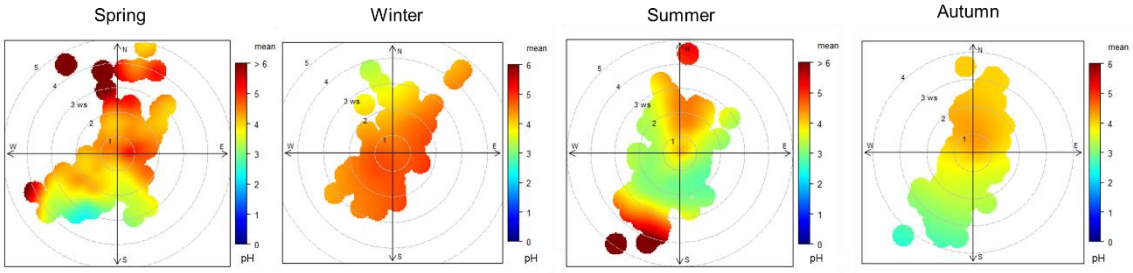

Figure 5.

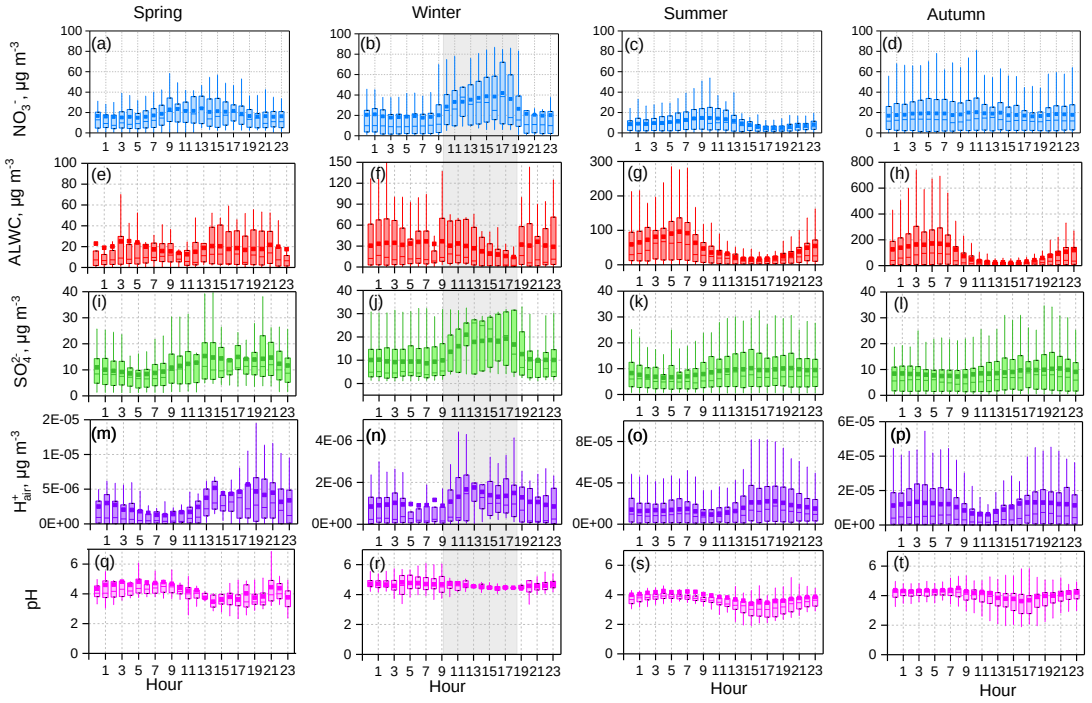

Figure 6.

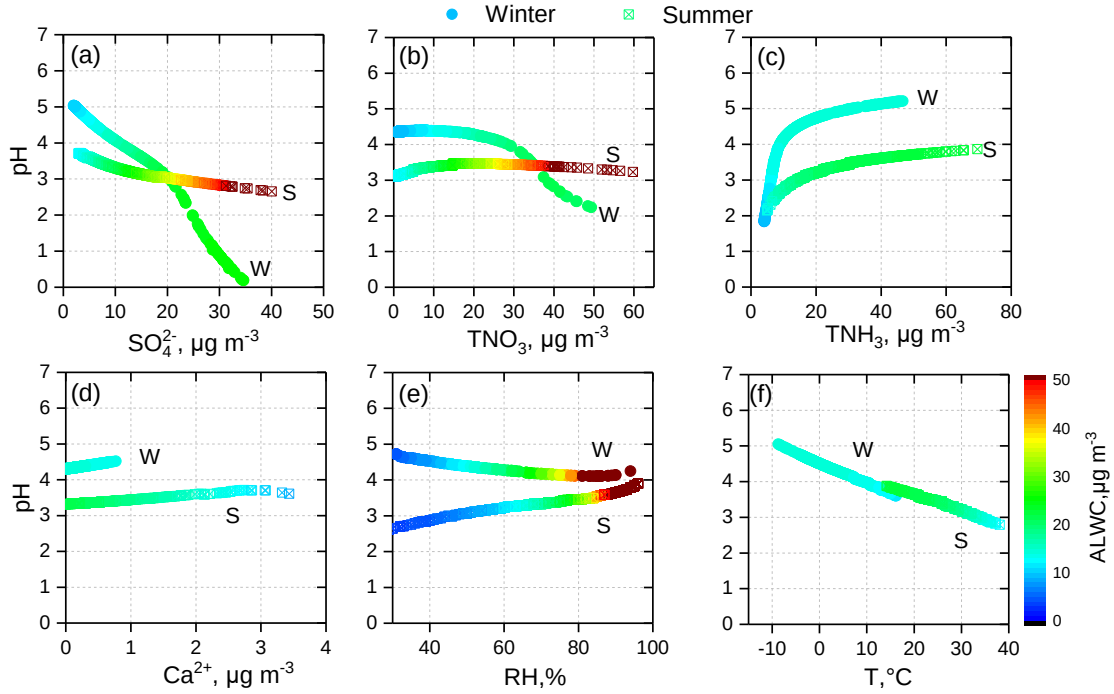

Figure 7.

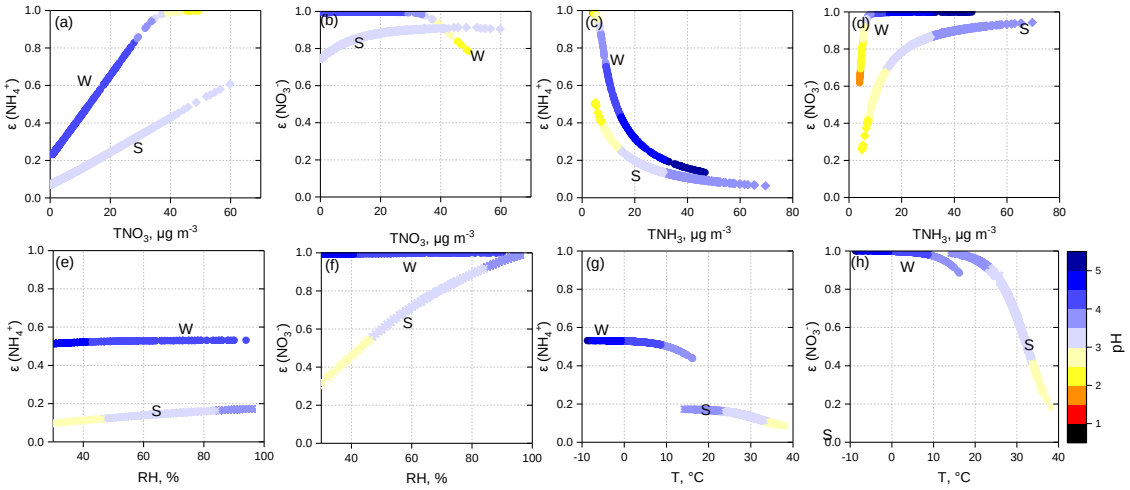

693
694
695 **Figure 8.**
696

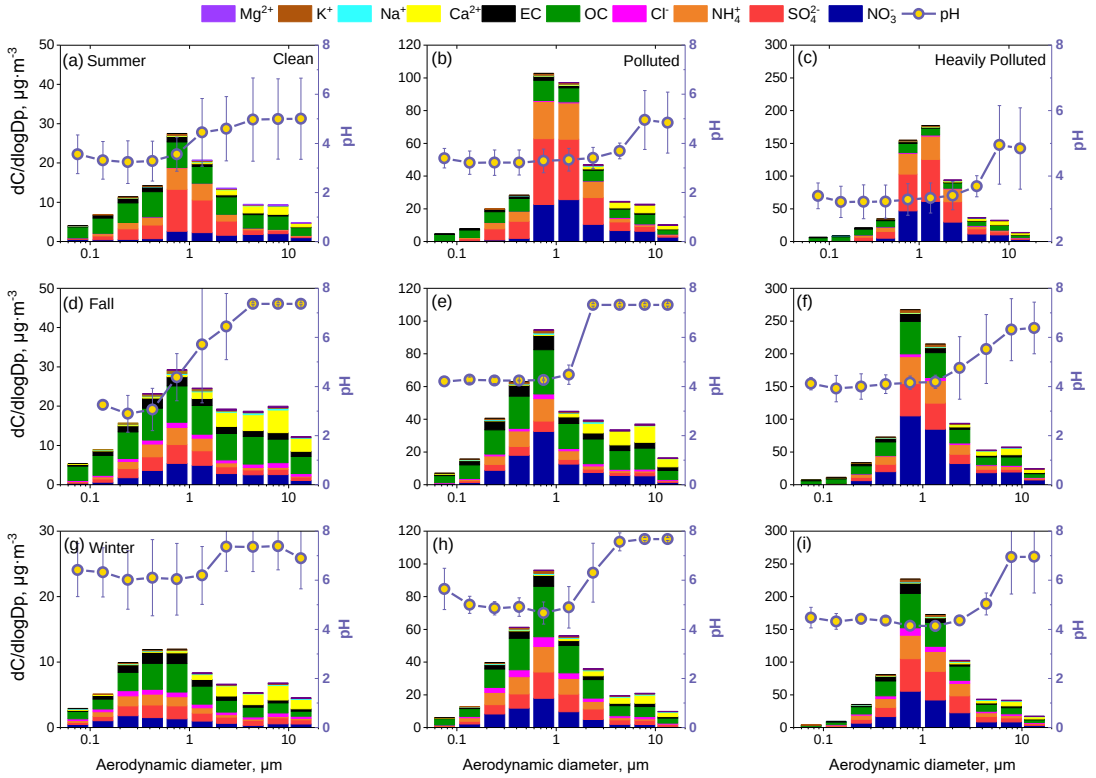

697
698 **Figure 9.**
699
700
701
702